Multiqubit matter-wave interferometry under decoherence and the Heisenberg scaling recovery

Yanming Che,[1] Jing Liu,[2] Xiao-Ming Lu,[3,*] and Xiaoguang Wang[1,†]

[1]*Zhejiang Province Key Laboratory of Quantum Technology and Device, Department of Physics, Zhejiang University, Hangzhou, Zhejiang 310027, China*

[2]*MOE Key Laboratory of Fundamental Physical Quantities Measurement & Hubei Key Laboratory of Gravitation and Quantum Physics, PGMF and School of Physics, Huazhong University of Science and Technology, Wuhan 430074, China*

[3]*Department of Physics, Hangzhou Dianzi University, Hangzhou, Zhejiang 310018, China*

(Received 17 August 2018; revised manuscript received 6 December 2018; published 4 March 2019)

Most matter-wave interferometry (MWI) schemes for quantum sensing have so far been evaluated in ideal situations without noise. In this work, we provide assessments of generic multiqubit MWI schemes under Markovian dephasing noise. We find that, for certain classes of the MWI schemes with scale factors that are nonlinearly dependent on the interrogation time, the optimal precision of maximally entangled probes *decreases* with increasing particle number N, for both independent and collective dephasing situations. This result challenges the conventional wisdom found in dephasing Ramsey-type interferometers. We initiate the analyses by investigating the optimal precision of multiqubit Sagnac atom interferometry for rotation sensing. And we show that, due to the competition between the unconventional interrogation-time quadratic phase accumulation and the exponential dephasing processes, the Greenberger–Horne–Zeilinger (GHZ) state, which is the optimal input state in noiseless scenarios, leads to vanishing quantum Fisher information in the large-N regime. Then our assessments are further extended to generic MWI schemes for quantum sensing with entangled states and under decoherence. Finally, a quantum error-correction logical GHZ state is tentatively analyzed, which could have the potential to recover the Heisenberg scaling and improve the sensitivity.

DOI: 10.1103/PhysRevA.99.033807

I. INTRODUCTION

Matter-wave interferometry (MWI) is sensitive to inertial effects and has been widely used in quantum sensing of physical quantities, including gravitational force, acceleration, and rotation of reference frames [1]. With quantum entanglement as resources, quantum sensing is expected to achieve higher precision and sensitivity; e.g., the Heisenberg limit [2,3]. Sagnac atom-interferometry gyroscopes (SAIGs) are quantum sensors for rotation frequency based on the Sagnac interferometry [4] of matter waves, where atoms are coherently split and controlled with wave guides (see, e.g., Ref. [5]) to enclose a finite area in space and encode the rotation frequency into the Sagnac phase, which can be finally read out from the interference fringes [4–11].

Most of schemes for SAIG utilize both the wave nature and spin degrees of freedom (hyperfine states) of atoms. For example, a scheme with uncorrelated and trap-guided atomic clocks was proposed in Ref. [12], and was later generalized to the one with a multiparticle Greenberger–Horne–Zeilinger (GHZ) state to beat the standard quantum limit (SQL) in Ref. [13]. So far, these proposed schemes were considered in ideal situations where the sensing protocols consisted of perfect unitary quantum channels. However, in realistic experiments, inevitable noise may cause errors which prevent the expected precision.

In standard Ramsey interferometers for atomic clocks, where the transition frequency ω between two energy levels of atoms is measured, the phase accumulation is linear in the interrogation time while the dephasing caused by noise is exponential. And the use of entangled states has been proved to only give a constant improvement for the ultimate precision, but still follows the SQL [14–16]. Several strategies and techniques have been proposed and used to protect the precision of atomic clocks from noise [17–21]. However, the evaluation and optimization of generic multiqubit MWI schemes for quantum sensing under decoherence still remain challenging.

In this paper, we present an assessment of generic MWI schemes with maximally entangled states and under dephasing noise. Starting with the SAIG as a prototype, we analyze the competition between the unconventional phase accumulation and the exponential dephasing processes. And we find that, for certain classes of the MWI schemes with scale factors that depend nonlinearly on the interrogation time, the optimal precision of maximally entangled probes *decreases* with increasing particle number N, for both independent and collective dephasing situations. These classes include most of the current mainstream MWI schemes with atomic clock states and certain time-dependently-controlled Hamiltonian systems. Our findings challenge the conventional wisdom found in dephasing Ramsey-type interferometers [14–16].

This paper is organized as follows: In Sec. II we model the matter-wave Sagnac interferometry with maximally entangled states and derive the multiparticle Sagnac phase. In Sec. III we evaluate the optimal sensitivity of Sagnac-type

*luxiaoming@gmail.com
†xgwang1208@zju.edu.cn

interferometers under local decoherence noise via the quantum Fisher information. In Sec. IV, we provide assessments of generic multiqubit MWI schemes with GHZ inputs and under independent Markovian dephasing noise. In Sec. V the QFI of generic multiqubit MWI schemes with GHZ inputs under collective dephasing is provided. In Sec. VI the potential of recovering the Heisenberg scaling with quantum error-correction codes is presented. Finally, in Sec. VII, we conclude our work and give further discussions on the minor enhancement by entanglement in the precision of Sagnac-type interferometers.

II. MATTER-WAVE SAGNAC INTERFEROMETRY WITH ENTANGLED STATES

To sense the rotation frequency of a reference frame $\mathcal{R}$ rotating at an angular velocity $\mathbf{\Omega}$ with respect to an inertial frame $\mathcal{K}$, N two-state cold atoms [22] can be initially prepared in the GHZ state (e.g., via the nonlinear [23–28] or Rydberg blockade [29] interactions with suitable coupling parameters), which is the optimal multiparticle input state for unitary quantum channels [30], i.e., $|\psi_0\rangle = (|\mathbf{0}\rangle + |\mathbf{1}\rangle)/\sqrt{2}$, where $|\mathbf{0}\rangle = |0\rangle^{\otimes N}$ and $|\mathbf{1}\rangle = |1\rangle^{\otimes N}$, with $|0\rangle = |\uparrow\rangle$ ($|1\rangle = |\downarrow\rangle$) being the single-atom (pseudo)spin state and eigenstate of the Pauli matrix σ_z with eigenvalue $+1$ (-1). Subsequently, the $|\mathbf{0}\rangle$ and $|\mathbf{1}\rangle$ components are coherently split by a beam splitter which establishes a state-path entanglement, and then are guided to transport along two distinct paths in real space [31], within an interrogation time τ, and are finally recombined at $t = \tau$. The state-path entanglement associates the phase shift between two interferometer paths (Sagnac phase) with the relative phase of two atomic states (qubit phase), which can be read out from the atomic spectroscopy; e.g., a parity measurement [13,23,32], after applying a $\pi/2$ pulse.

A. Model.

We assume that the N two-state bosonic atoms are in the Bose–Einstein condensed (BEC) state, which is described by the mean-field wave function (order parameter) $\Psi_\xi(\mathbf{r}, t)$ for the two split components $|\xi\rangle = |0\rangle$ and $|\xi\rangle = |1\rangle$, respectively. And the wave guide is provided by a ring trap of toroidal geometry [7,9,10,33], with a trapping potential in cylindrical coordinates $\{r, \theta, z\}$ of the form $V_{\rm trap}(\mathbf{r}, t) = \frac{1}{2}m[\omega_r^2(r-R)^2 + \omega_\theta^2 R^2\theta^2\Theta(-t) + \omega_z^2 z^2]$ [7,10], where m is the particle mass and $(\omega_r, \omega_\theta, \omega_z)$ are the respective (radial, angular, axial) trapping frequencies, and $\Theta(-t)$ and R are the Heaviside step function and the radius of the circular interferometer, respectively. See Fig. 1 for a schematic illustration, where we assume $\mathbf{\Omega} = \Omega\mathbf{z}$. When the radial and axial trapping confinements are sufficiently tight, the dynamics along these directions is freezed and then the time evolution ($t \geqslant 0$) of the order parameter in the rotating frame $\mathcal{R}$ is given by the one-dimensional Gross–Pitaevskii (GP) equation [34]

$$i\hbar\frac{\partial}{\partial t}\Psi_\xi(\theta, t) = H_\xi\Psi_\xi(\theta, t), \tag{1}$$

with the mean-field Hamiltonian

$$H_\xi = \frac{\hat{L}_z^2}{2mR^2} + \mathcal{U}|\Psi_\xi(\theta, t)|^2 - \Omega\hat{L}_z, \tag{2}$$

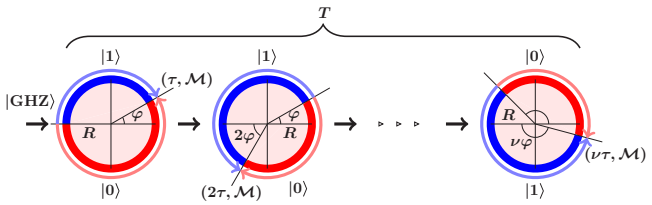

FIG. 1. Schematic matter-wave Sagnac interferometer for rotation sensing with entangled GHZ input of BEC atoms and circular waveguides of radius R in the x-y plane, observed from the inertial frame $\mathcal{K}$. The $|\mathbf{0}\rangle$ (red) and $|\mathbf{1}\rangle$ (blue) components are coherently split at $t = 0$ and then are counter-transported along the two interferometer paths. Finally they are recombined at time $t = \tau$, where a $\pi/2$ pulse and measurement $\mathcal{M}$ are performed to read out the encoded rotation frequency. The above process is repeated for $\nu = T/\tau$ times to achieve a high precision. The tuple at the end of each period denotes (time, measurement). The reference frame rotates with an angular velocity $\mathbf{\Omega} = \Omega\mathbf{z}$ and $\varphi = \Omega\tau$.

where $\hat{L}_z = -i\hbar\frac{\partial}{\partial\theta}$ is the axial angular-momentum operator and $\mathcal{U}$ is the contact-interaction strength.

For the $\mathcal{U} = 0$ case, the time evolution operator for the ith particle reads

$$\hat{U}_i(t) = \exp\left(\Omega t\frac{\partial}{\partial\theta_i}\right)\exp\left[\frac{i\hbar t}{2mR^2}\frac{\partial^2}{\partial\theta_i^2}\right]\otimes\mathcal{I}_2, \tag{3}$$

where $\mathcal{I}_2$ is the two-dimensional identity matrix. The trapping potential along the angular direction is $V_{\rm trap}(\theta, t) = \frac{1}{2}m\omega_\theta^2R^2\theta^2\Theta(-t)$, and we assume that, for the both components, the initial mean-field wave function at $t = 0$ is a Gaussian wave packet, i.e., the ground state of the harmonic trap, $\Psi(\theta, 0) = (\frac{1}{\sqrt{\pi}\sigma})^{\frac{1}{2}}\exp\{-\frac{[\theta-\theta(0)]^2}{2\sigma^2}\}$ for $\theta \in [\theta(0) - \pi, \theta(0) + \pi]$, where $\theta(0) = 0$ and $\sigma = \sqrt{\hbar/(m\omega_\theta)}/R \ll \pi$ are the initial center and the width of the wave packet, respectively. Due to the periodicity of the θ coordinate, the wave function outside this interval can be defined via $\Psi(\theta + 2J\pi, 0) = \Psi(\theta, 0)$, with J being an integer. The multiqubit initial GHZ state, is given by

$$|\tilde{\psi}(\theta_1, \theta_2, \ldots, \theta_N; 0)\rangle = \frac{1}{\sqrt{2}}\prod_{i=1}^{N}\Psi(\theta_i, 0)(|\mathbf{0}\rangle + |\mathbf{1}\rangle), \tag{4}$$

for which the normalization condition is $1 = \int d\theta_1 d\theta_2\cdots d\theta_N\langle\tilde{\psi}(\theta_1, \theta_2, \ldots, \theta_N; 0)|\tilde{\psi}(\theta_1, \theta_2, \ldots, \theta_N; 0)\rangle$. The interferometer is launched at $t = 0$ via kicking the two components with $\pm v$ group velocity, respectively, as in Refs. [7,10]. The kicking operator reads $\hat{K}(v) = \exp(\frac{i}{\hbar}L_k\sum_{j=1}^{N}\theta_j\sigma_{jz})$, which plays the role of a beam splitter, with $L_k = mRv$ being the kicking angular momentum and σ_{jz} being the Pauli Z matrix of the jth particle. Finally, at time $t = \tau$ when the two components are recombined for the first time [35], the full quantum state is given by

$$|\tilde{\psi}(\theta_1, \theta_2, \ldots, \theta_N; \tau)\rangle = \hat{K}^\dagger(v)\bigotimes_{i=1}^{N}\hat{U}_i(\tau)\hat{K}(v) \times|\tilde{\psi}(\theta_1, \theta_2, \ldots, \theta_N; 0)\rangle, \tag{5}$$

where $\hat{U}_i(\tau)$ is the time evolution operator for the ith qubit at $t=\tau$, which is given by Eq. (3). Note that, for a well defined Sagnac phase, we have first to assume the interaction $\mathcal{U}=0$ during the interrogation. Consequently, the quantum state in the spin subspace after tracing out the orbital degrees of freedom related to $\Psi_\xi(\theta,\tau)$ is given by $|\psi(\tau)\rangle=(e^{i\phi_S}|\mathbf{0}\rangle+|\mathbf{1}\rangle)/\sqrt{2}$ (up to a global phase factor), where (see Appendix A for detailed derivations)

$$\phi_S=\beta N\Omega\tau^2 \tag{6}$$

is the multiparticle Sagnac phase, with $\beta=2mv^2/(\pi\hbar)$. This expression for ϕ_S is equivalent to N times the well-known single-particle Sagnac phase $2m\Omega A/\hbar$, where $A=\pi R^2$ is the area of the Sagnac interferometer, and for constant v we have $A=v^2\tau^2/\pi$.

As a result, a Sagnac pure phase gate as a unitary operation mapping the initial state of the qubits to the readout state is constructed, which in the GHZ subspace spanned by $\{|\mathbf{0}\rangle,|\mathbf{1}\rangle\}$ reads

$$U(\phi_S)=\mathrm{diag}[e^{i\phi_S},1], \tag{7}$$

and the rotation frequency can be extracted from the interference signal of the final state. Following standard quantum metrological protocols, the above Sagnac phase encoding and rotation frequency readout processes are repeated for $\nu=T/\tau$ times to reach a high precision, where T is the total resource time (see Fig. 1). And the standard deviation $\delta\hat{\Omega}$ for any unbiased estimator $\hat{\Omega}$ of the rotation frequency is bounded from below by the quantum Cramér–Rao bound (QCRB) [36,37], $\delta\hat{\Omega}\geqslant 1/\sqrt{\nu F}$, where F is the quantum Fisher information (QFI) with respect to Ω for the readout state, which is an effective theoretical tool for assessing the performance of various interferometry schemes for quantum sensing [10]. Equivalently, we have $\delta\hat{\Omega}\sqrt{T}\geqslant 1/\sqrt{F/\tau}$. For more introduction to quantum sensing and QFI, see Appendix B. From Eq. (6), we see that the scale factor $\mathcal{S}$ of the interferometer is $\mathcal{S}\propto N\tau^2$, and the noiseless optimal QFI is [13]

$$F_0=(\partial_\Omega\phi_S)^2=(2mNA/\hbar)^2, \tag{8}$$

which achieves the Heisenberg scaling and increases monotonically with the area of the interferometer.

III. OPTIMAL SENSITIVITY UNDER INDEPENDENT DECOHERENCE

In previous derivations of the multiqubit Sagnac phase we neglected the interaction and local field fluctuations. Now we consider the qubit dephasing arising from such effects, which cannot be neglected in a realistic system [38]. And for shortcomings of the mean-field analysis in MWI with interaction effects; see, e.g., Refs. [39,40]. The atom-atom collision and local fluctuations may cause a random shift $\delta\omega(t)$ of the energy difference for each qubit, which can be formulated as a Gaussian random process with zero mean and the correlation function [41,42] $\langle\delta\omega(t)\delta\omega(t')\rangle=2\gamma\delta(t-t')$, where $\delta(t-t')$ is the Dirac function. The ensemble average leads to the exponential dephasing of the single qubit [41,43,44]. Considering the dephasing of the N-qubit system, the master equation for the state $\varrho(t)$ in the phase-covariant frame can be written as [45]

$$\frac{d\varrho(t)}{dt}=\frac{\gamma}{2}\sum_{i=1}^{N}[\sigma_{iz}\varrho(t)\sigma_{iz}-\varrho(t)], \tag{9}$$

where $\gamma>0$ is the dephasing strength.

The completely positive and trace preserving (CPTP) map $\mathcal{E}$, which is a solution of Eq. (9) and maps ϱ_0 to $\varrho(\tau)$, is $\varrho(\tau)=\mathcal{E}(\varrho_0)=\bigotimes_{i=1}^{N}\mathcal{E}_i(\varrho_0)$, where $\varrho_0=\rho_0=|\psi_0\rangle\langle\psi_0|$ is the initial state and $\mathcal{E}_i(\varrho_0)=E_{i0}\varrho_0E_{i0}^\dagger+E_{i1}\varrho_0E_{i1}^\dagger$ is the local phase-flip error operator for the ith qubit, with $E_{i0}=\sqrt{1-p(\tau)}\mathcal{I}_2$ and $E_{i1}=\sqrt{p(\tau)}\sigma_{iz}$ being the Kraus operators, where $p(\tau)=(1-e^{-\gamma\tau})/2$ is the single-qubit error probability. Then it is straightforward to reach the readout state [46], $\rho(\tau)=\mathcal{E}[U(\phi_S)\rho_0U^\dagger(\phi_S)]=[|\mathbf{0}\rangle\langle\mathbf{0}|+|\mathbf{1}\rangle\langle\mathbf{1}|+(e^{-N\gamma\tau}e^{i\phi_S}|\mathbf{0}\rangle\langle\mathbf{1}|+\mathrm{H.c.})]/2$, where ϕ_S is given by Eq. (6). The QFI with respect to Ω for this state is (see Appendix C)

$$F=\beta^2N^2\tau^4e^{-2N\gamma\tau}. \tag{10}$$

Note that here, F is the interrogation-time-dependent QFI at the point where the Sagnac phase accumulation is accomplished, which is actually F_S in Ref. [10]. From Eq. (10) we see that the optimal interrogation time and the Sagnac area A are constrained by decoherence in noisy scenarios.

The precision bound for rotation sensing is determined by F/τ and its optimized value over the interrogation time is given by

$$(F/\tau)_{\mathrm{opt}}=\beta^2\left(\frac{3}{2\gamma e}\right)^3\frac{1}{N}, \tag{11}$$

with $\tau_{\mathrm{opt}}=3/(2N\gamma)$ [47]. Therefore, the maximally entangled state reduces the precision with increasing N even under uncorrelated dephasing, which is a completely new result in contrast to that was found in Ramsey-type interferometers [14–16]. On the other hand, the QFI for uncorrelated qubits is given by $F_{\mathrm{SQL}}=N\beta^2\tau^4e^{-2\gamma\tau}$ and is proportional to N for any value of τ. Shown in Fig. 2 is the interrogation-time normalized F for increasing the qubit number N with GHZ probe [Fig. 2(a)] and uncorrelated qubits [Fig. 2(b)], respectively. For a given value of N and increasing τ, the power law τ^3 behavior dominates at the beginning while the exponential prevails after reaching a maximum. While the SQL is achieved in Fig. 2(b) with uncorrelated qubits, in contrast, the QFI curves are shrinking with increasing N in Fig. 2(a) for the GHZ probe. The physical reason is that $\phi_S(\tau=\tau_{\mathrm{opt}})\propto N^{-1}$, such that the accumulated phase signal is weakened with increasing N.

IV. ASSESSMENTS OF GENERIC MULTIQUBIT MATTER-WAVE-INTERFEROMETRY SCHEMES

The results above can be generalized to more generic MWI schemes for quantum sensing with entangled states and under independent dephasing, which were previously only considered in single-qubit or noiseless scenarios. In general, for GHZ probes in the presence of independent dephasing, if the accumulated phase is $\phi_\chi(\tau)\propto N\chi\tau^\lambda$ with χ being the physical quantity to be sensed and $\lambda>0$ the time exponent of

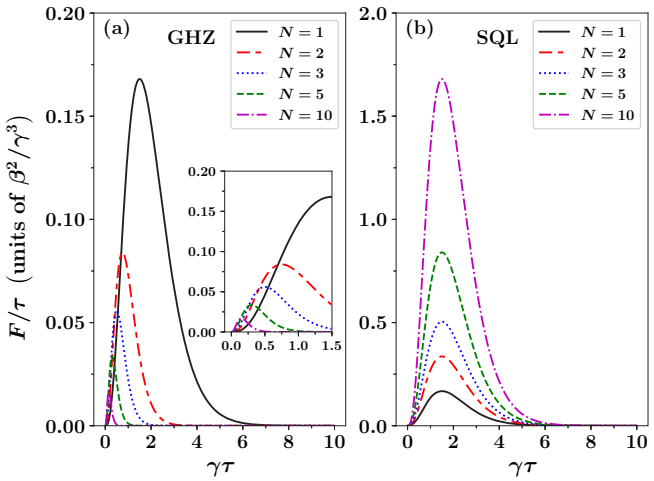

FIG. 2. The QFI F/τ (in units of β^2/γ^3) of Sagnac interferometers as functions of $\gamma\tau$ for increasing the qubit number N with (a) GHZ probe and (b) uncorrelated qubits, where SQL represents the standard quantum limit and $F_{\rm SQL}/\tau = N\beta^2\tau^3 e^{-2\gamma\tau}$. The inset in panel (a) presents the detailed structure near the optimal interrogation time $\tau_{\rm opt}$ and shares the same axes with the main panel (a). For panel (a), both $(F/\tau)_{\rm opt}$ and $\tau_{\rm opt}$ are proportional to N^{-1}, and the QFI is completely lost in the large-N region. In panel (b), $\tau_{\rm opt}$ = const. and $(F_{\rm SQL}/\tau) \propto N$ (SQL). Note that the black solid lines in panels (a) and (b) represent exactly the same function.

the scale factor, then the optimal QFI with respect to χ is

$$(F_\chi/\tau)_{\rm opt} = O(N^{3-2\lambda}), \tag{12}$$

with $\tau_{\rm opt} = (2\lambda-1)/(2N\gamma)$ (see Appendix C). Therefore, we may conclude that the Heisenberg scaling is actually inaccessible because the condition $\tau_{\rm opt} > 0$ requires $\lambda > 1/2$. And for $\lambda \geqslant 1$, the best QFI that can be achieved is $(F_\chi/\tau)_{\rm opt} = O(N)$ (SQL) with the $\lambda = 1$ class [14–16]. For classes with $\lambda \geqslant 2$, the entangled probes could reduce the precision with increasing the particle number.

Many of the current mainstream MWI schemes with atomic clock states belong to the $\lambda = 2$ class (without entanglement), and so do the proposed schemes in Refs. [48,49] with time-dependently controlled Hamiltonians. For example, the atom gravimetry considered in Refs. [5,50–53], with the single-qubit phase $\phi_{\mathbf{g}}(\tau) = \mathbf{k}_0 \cdot \mathbf{g}(\tau/2)^2$ and the atom free-propagation Sagnac interferometers in Refs. [4,6,54,55], with the encoded phase $\phi_{\mathbf{\Omega}}(\tau) = \mathbf{k}_0 \cdot (\mathbf{v}_0 \times \mathbf{\Omega})\tau^2/2$, where $\mathbf{g}$ is gravitational acceleration, and $\mathbf{v}_0$ and $\mathbf{k}_0$ are the semiclassical velocity of atoms and effective Raman propagation vectors, respectively. In Table I we give a comparison between standard Ramsey interferometers for atomic clocks ($\lambda = 1$) and Sagnac interferometers for rotation sensing ($\lambda = 2$) [56], with GHZ input states and $H_{\rm single}$ denoting the single-particle sensing Hamiltonian.

V. QUANTUM FISHER INFORMATION IN THE PRESENCE OF COLLECTIVE DEPHASING

For closely spaced atoms in a Bose–Einstein condensate, they may collectively couple to the external-field fluctuations [42,57–59]. Here we give the scaling behavior the QFI in the presence of collective dephasing for matter-wave interferometers with a GHZ probe and different scale factors.

The master equation for the state $\varrho(t)$ in the phase-covariant frame in the presence of collective dephasing is given by [58,59]

$$\frac{d\varrho(t)}{dt} = \Gamma\left[2J_z\varrho(t)J_z - J_z^2\varrho(t) - \varrho(t)J_z^2\right], \tag{13}$$

where $\Gamma > 0$ is the collective dephasing strength and $J_z = \sum_{i=1}^{N}\sigma_{iz}/2$ is the third component of the collective spin operator. For the GHZ state, the readout state at time $t = \tau$ can be analytically calculated in a similar way, which is given by

$$\rho(\tau) = \tfrac{1}{2}[|\mathbf{0}\rangle\langle\mathbf{0}| + |\mathbf{1}\rangle\langle\mathbf{1}| + (e^{-N^2\Gamma\tau}e^{i\phi(\tau)}|\mathbf{0}\rangle\langle\mathbf{1}| + \text{H.c.})], \tag{14}$$

where ϕ is the multiparticle interferometer phase $\phi(\tau) \propto N\chi\tau^\lambda$ with the scale factor $\mathcal{S} \propto N\tau^\lambda$. The QFI with respect to χ for this state can be calculated with the same method as in Appendix C and is given by

$$\mathcal{F}_\chi = \left[\frac{\partial\phi(\tau)}{\partial\chi}\right]^2 e^{-2N^2\Gamma\tau} = \mathcal{S}^2 e^{-2N^2\Gamma\tau} \propto N^2\tau^{2\lambda}e^{-2N^2\Gamma\tau}. \tag{15}$$

And the interrogation-time optimized value of $\mathcal{F}_\chi/\tau$ is

$$(\mathcal{F}_\chi/\tau)_{\rm opt} \propto N^{4(1-\lambda)}\left(\frac{2\lambda-1}{2\Gamma e}\right)^{2\lambda-1}, \tag{16}$$

with $\tau_{\rm opt} = (2\lambda-1)/(2N^2\Gamma)$. So for Ramsey-type interferometers ($\lambda = 1$), the optimal QFI is $(\mathcal{F}_\chi/\tau)_{\rm opt} = 1/(2\Gamma e) =$ const. [42,58,59] and is independent of N. While for Sagnac-type interferometers with $\lambda = 2$, the decoherence time is $\tau_{\rm opt} \propto N^{-2}$ and $(\mathcal{F}_\chi/\tau)_{\rm opt} \propto N^{-4}[3/(2\Gamma e)]^3$, which decreases very rapidly with increasing the particle number N. This is in stark contrast to the constant precision of Ramsey-type interferometers [42,58,59].

VI. RECOVERING THE HEISENBERG SCALING WITH QUANTUM ERROR CORRECTION

To tentatively recover the Heisenberg scaling and improve the sensitivity, we theoretically explore in the following the potential of quantum error-correction (QEC) codes for MWI

TABLE I. Comparison between Ramsey and Sagnac interferometers with GHZ probe states.

Interferometers	Quantity	$H_{\rm single}$	Phase	Noiseless F/τ	Noiseless $\tau_{\rm opt}$	Dephasing	Noisy $(F/\tau)_{\rm opt}$	Noisy $\tau_{\rm opt}$
Ramsey	ω	$\hbar\omega\sigma_z/2$	$N\omega\tau$	$O(N^2)$	T	$e^{-N\gamma\tau}$	$O(N)$ [14–16]	$1/(2N\gamma)$
Sagnac	Ω	$-\Omega\hat{L}_z$	$\beta N\Omega\tau^2$	$O(N^2)$ [13]	T	$e^{-N\gamma\tau}$	$O(N^{-1})$	$3/(2N\gamma)$

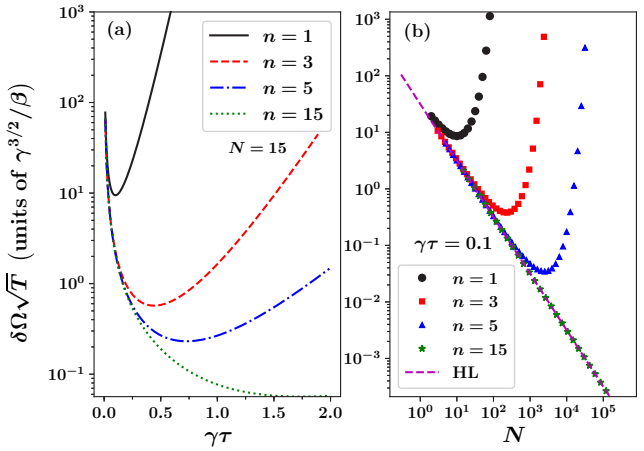

FIG. 3. The QCRB $\delta\Omega\sqrt{T} = 1/\sqrt{F_L/\tau}$ (in units of $\gamma^{3/2}/\beta$) for rotation frequency sensing. (a) $\delta\Omega\sqrt{T}$ vs $\gamma\tau$ for fixed total qubit number $N = 15$ and (b) $\delta\Omega\sqrt{T}$ vs N for $\gamma\tau = 0.1$, with increasing the number of qubits n in each logical block. HL in panel (b) denotes the Heisenberg limit (magenta dashed). See main text for details.

schemes under local dephasing. QECs have been realized in experiments for quantum computation [21,60–62] and have been proposed for quantum metrology [19,20,63–68]. Here we analyze a QEC scheme with logical GHZ states proposed in Refs. [20,64], which utilizes redundant qubits to suppress phase-flip errors, with a possible application in the Sagnac atom interferometers. As in Refs. [20,64], with n physical qubits in each logical block, the error probability $p(\tau)$ is exponentially suppressed by replacing the raw GHZ state with a logical one [20,64], where the coding space $\mathcal{C}(\mathcal{G})$ is stabilized by the stabilizer group $\mathcal{G}$. The n-qubit (n is odd) phase-flip code is defined as $\mathcal{C}_n = \{|0\rangle_L, |1\rangle_L\}$, where $|0\rangle_L = (|+\rangle^{\otimes n} + |-\rangle^{\otimes n})/\sqrt{2}$ and $|1\rangle_L = (|+\rangle^{\otimes n} - |-\rangle^{\otimes n})/\sqrt{2}$ are the bases for each logical qubit block, with $|+\rangle$ ($|-\rangle$) being the eigenstate of the Pauli matrix σ_x with eigenvalue $+1$ (-1). The above code is stabilized by the operator $X_\alpha = \prod_{i\in\alpha}\sigma_{ix}$, with $\alpha \subset \{1, 2, 3, \ldots n\}$ and $|\alpha| =$ even, and is capable of correcting $(n-1)/2$ phase-flip errors $\{\sigma_{iz}\}$ [20,64]. With N total physical qubits as resources, the number of logical qubits is N/n. Furthermore, the error probability is renormalized to the logical level as

$$p_L(\tau) = \sum_{k=0}^{(n-1)/2} \binom{n}{k} p^{n-k}(\tau)[1-p(\tau)]^k. \tag{17}$$

The QFI can be rewritten in terms of $p(\tau)$ by using $e^{-\gamma\tau} = 1 - 2p(\tau)$, and the logical QFI in terms of $p_L(\tau)$ is given by

$$\begin{aligned} F_L &= (n\beta)^2(N/n)^2\tau^4[1-2p_L(\tau)]^{2N/n} \\ &= \beta^2 N^2\tau^4[1-2p_L(\tau)]^{2N/n}. \end{aligned} \tag{18}$$

Now the quantum Crámer–Rao bound for the rotation frequency sensing is $\delta\Omega\sqrt{T} = 1/\sqrt{F_L/\tau}$.

Plotted in Fig. 3(a) is $\delta\Omega\sqrt{T}$ vs $\gamma\tau$ for a given total qubit number $N = 15$ and increasing qubit number n in each logical block. With small $p(\tau)$, the optimal interrogation time which minimizes the precision bound is $\tau_{\rm opt} = 3/(2N\gamma_{\rm eff})$, as in Eq. (11), with the effective dephasing strength $\gamma_{\rm eff} = \gamma O[p^{(n-1)/2}(\tau_{\rm opt})]$. We find that the use of the logical code will increase $\tau_{\rm opt}$ in a power-law fashion and improve the sensitivity, where the preservation of Heisenberg scaling is promising. Shown in Fig. 3(b) is $\delta\Omega\sqrt{T}$ vs N for $\gamma\tau = 0.1$. The representative values for n are taken to be the same as in Fig. 3(a). One sees that, for each n, there exists an optimal total qubit number $N_{\rm opt}$, where a minimum precision bound is attained. Furthermore, for $N \in [1, N_{\rm opt})$, the Heisenberg scaling (shown with magenta dashed) is achieved [20]. For small $\gamma\tau$ and $p(\tau)$, it is straightforward to obtain $N_{\rm opt} = {\rm int}\{1/[2p_L + O(p_L^2)]\}n$, where int$\{y\}$ denotes the integer part of y. For the set of values of n and $\gamma\tau$ in Fig. 3(b), $N_{\rm opt} \approx (10, 219, 2320, 4.5\times10^7)$ for $n = (1, 3, 5, 15)$, respectively. Therefore, with the help of the logical code, the effective scope for the Heisenberg scaling can be extended.

VII. CONCLUSION AND DISCUSSION

In summary, we have presented an assessment of the optimal precision given by the QCRB for matter-wave interferometers, with multiqubit GHZ input and in the presence of decoherence. Our results show that, due to the competition between the unconventional phase accumulation (i.e., $\lambda \geqslant 2$) and the exponential dephasing, the use of entangled probes leads to vanishingly small QFI while increasing the particle number, which challenges the conventional wisdom. Finally, for completeness, we tentatively analyzed a QEC scheme with logical GHZ states, which could have the potential to protect the Heisenberg scaling.

It is worth noting that the nonentangled spin state and maximally entangled GHZ state with unconventional interferometric scale factors are investigated and compared in our work, due to the analytical computability of the QCRB for such states. We show that the latter gives a much worse precision than the former for Sagnac-type interferometers in the presence of uncorrelated dephasing. Intuitively, there should be a maximal precision arising from the balance between the entanglement-enhancement and noise-reduction effects. With the general method in Ref. [15] for estimating the upper bound of the noisy QFI maximized over all possible input states and by replacing the scale factor $\mathcal{S} \propto \tau$ of Ramsey-type interferometers with $\mathcal{S} \propto \tau^2$, one can obtain that the use of (partially) entangled states can only give 2.8% relative precision enhancement with respect to the uncorrelated spin state for Sagnac interferometers. This is quite minor compared with the $\sqrt{e}$ enhancement in Ramsey-type interferometers [14–16].

ACKNOWLEDGMENTS

We acknowledge helpful discussions with Jun Xin and Hui–Ke Jin. This work was supported by the National Key Research and Development Program of China (Grants No. 2017YFA0304202 and No. 2017YFA0205700), the NSFC through Grant No. 11875231, and the Fundamental Research Funds for the Central Universities through Grant No. 2018FZA3005. J. Liu acknowledges the support from the National Natural Science Foundation of China (Grant No.11805073). X.M. Lu acknowledges support from the National Natural Science Foundation of China under Grants No. 61871162 and No. 11805048, and the Natural

Science Foundation of Zhejiang Province under Grant No. LY18A050003.

APPENDIX A: DERIVATION OF THE MULTIQUBIT SAGNAC PHASE IN EQ. (6)

Here we provide detailed derivation of the multiqubit Sagnac phase in Eq. (6) in the main text. After applying the kicking operator $\hat{K}(v)$, the mean-field wave function for the jth particle of $|\xi\rangle_j$ spin state ($\xi = 0, 1$) is given by $\Psi_\xi(\theta_j, 0) = \Psi(\theta_j, 0)\exp[(-1)^\xi iL_k\theta_j/\hbar]$, which can be directly obtained with $\sigma_{jz}|\xi\rangle_j = (-1)^\xi|\xi\rangle_j$, and $\Psi(\theta_j, 0)$ is the initial Gaussian wave packet. Therefore, the wave function at time t reads

$$\Psi_\xi(\theta_j, t)\otimes|\xi\rangle_j = \hat{U}_j(t)\Psi_\xi(\theta_j, 0)\otimes|\xi\rangle_j. \tag{A1}$$

In addition, the Fourier transform of the initial Gaussian wave packet is given by $\Psi(\theta, 0) = [1/(2\pi)]^{1/2}\sum_{l=-\infty}^{l=+\infty}\tilde{\Psi}(l)\exp(il\theta)$, where

$$\begin{aligned}\tilde{\Psi}(l) &= [1/(2\pi)]^{1/2}\int_{-\pi}^{\pi}\Psi(\theta, 0)\exp(-il\theta)d\theta\\ &= (\sigma/\sqrt{\pi})^{1/2}\exp(-\sigma^2l^2/2)\mathrm{erf}\left(\frac{\pi + i\sigma^2l}{\sqrt{2}\sigma}\right)\\ &\approx (\sigma/\sqrt{\pi})^{1/2}\exp(-\sigma^2l^2/2),\end{aligned} \tag{A2}$$

where $\mathrm{erf}(z) = \frac{2}{\sqrt{\pi}}\int_0^z\exp(-t^2)dt$ is the Gaussian error function, for which $\mathrm{erf}(z)\to 1$ when $\mathrm{Re}\,z\to+\infty$, which is the situation with $\sigma \ll \pi$ here. And by applying the time evolution operator $\hat{U}_j(t)$, one can obtain

$$\begin{aligned}\Psi_\xi(\theta_j, t) \approx& \left(\frac{1}{\sqrt{\pi}\tilde{\sigma}(t)}\right)^{\frac{1}{2}}\exp\left\{-\frac{[\theta_j - \theta^{(\xi)}(t)]^2}{2\sigma\tilde{\sigma}(t)}\right\}\\ &\times\exp\left[(-1)^\xi\frac{i}{\hbar}L_k(\Omega t + \theta)\right]\exp\left[\frac{-itL_k^2}{2\hbar mR^2}\right]\\ &\times\sum_{n=-\infty}^{+\infty}\exp\{2\pi in\kappa - 2\pi^2n^2/[\sigma\tilde{\sigma}(t)]\},\end{aligned} \tag{A3}$$

where $\tilde{\sigma}(t) = \sigma + i\hbar t/(mR^2\sigma)$ and $\theta^{(\xi)}(t) = [(-1)^\xi v/R - \Omega]t$, and $\kappa = -i[\theta_j - \theta^{(\xi)}(t)]/[\sigma\tilde{\sigma}(t)]$. Furthermore, under the condition $|\tilde{\sigma}(t)| \ll \pi$ for $t\in[0,\tau]$, we have $\sum_{n=-\infty}^{+\infty}\exp\{2\pi in\kappa - 2\pi^2n^2/[\sigma\tilde{\sigma}(t)]\} = 1 + \sum_{n=-\infty, n\neq 0}^{+\infty}\exp\{2\pi in\kappa - 2\pi^2n^2/[\sigma\tilde{\sigma}(t)]\}\approx 1$, and then we obtain

$$|\Psi_\xi(\theta_j, t)|^2 \approx \frac{1}{\sqrt{\pi}|\tilde{\sigma}(t)|}\exp\left\{-\frac{[\theta_j - \theta^{(\xi)}(t)]^2}{|\tilde{\sigma}(t)|^2}\right\}. \tag{A4}$$

Therefore, at time t and under the condition $|\tilde{\sigma}(t)| \ll \pi$, the wave function in Eq. (A3) describes Gaussian wave packets centered at $\theta^{(\xi)}(t)$, i.e., propagating in group linear velocity $(-1)^\xi v - \Omega R$, for $\xi = 0$ and 1, respectively, and with the same width $|\tilde{\sigma}(t)|$. The interrogation time (or collision time) τ, at which the two centers of the counterpropagating Gaussian wave packets are completely overlapped, is given by $\theta^{(0)}(\tau) - \theta^{(1)}(\tau) = 2\pi$ or, equivalently, $\tau = \pi R/v$.

With above results, one can obtain the multiparticle readout state $|\tilde{\psi}(\theta_1, \theta_2, \ldots, \theta_N; \tau)\rangle$ in Eq. (5) and the corresponding density matrix reads $\tilde{\rho}(\theta_1, \theta_2, \ldots, \theta_N; \tau) = |\tilde{\psi}(\theta_1, \theta_2, \ldots, \theta_N; \tau)\rangle\langle\tilde{\psi}(\theta_1, \theta_2, \ldots, \theta_N; \tau)|$. The reduced density matrix in the spin subspace after tracing out the orbital degrees of freedom related to $\Psi_\xi(\theta, \tau)$ is given by

$$\begin{aligned}\rho(\tau) &= \int d\theta_1 d\theta_2\cdots d\theta_N\tilde{\rho}(\theta_1, \theta_2, \ldots, \theta_N; \tau)\\ &= \frac{1}{2}[|\mathbf{0}\rangle\langle\mathbf{0}| + |\mathbf{1}\rangle\langle\mathbf{1}| + (e^{i\phi_S}|\mathbf{0}\rangle\langle\mathbf{1}| + \mathrm{H.c.})],\end{aligned} \tag{A5}$$

where

$$\phi_S = \beta N\Omega\tau^2 \tag{A6}$$

is the multiparticle Sagnac phase, with $\beta = 2mv^2/(\pi\hbar)$. This expression for ϕ_S is equivalent to N times the well-known single-particle Sagnac phase $2m\Omega A/\hbar$, where $A = \pi R^2$ is the area of the Sagnac interferometer, and for constant v we have $A = v^2\tau^2/\pi$. The corresponding spin-subspace quantum state can be written as $|\psi(\tau)\rangle = (e^{i\phi_S}|\mathbf{0}\rangle + |\mathbf{1}\rangle)/\sqrt{2}$ (up to a global phase factor), with which $\rho(\tau)$ can be given by $\rho(\tau) = |\psi(\tau)\rangle\langle\psi(\tau)|$.

APPENDIX B: QUANTUM SENSING AND QUANTUM FISHER INFORMATION

Here we present a brief introduction to quantum sensing and QFI. The QFI plays a crucial role in quantum metrology and quantum sensing. Our basic quantum resources for a SAIG include N cold probe (two-level) atoms (qubits), a total sensing time T, single-round interrogation time τ, and the controlling and measurement devices. In a standard metrological scheme, the initial state of the probe is prepared at ρ_0 and followed by a dynamical evolution $\rho_0\xrightarrow{\phi_\chi(t)}\rho_\chi$ [$\rho_\chi := \rho_\chi(t)$], which encodes the quantity χ to be sensed into the relative phase $\phi_\chi(t)$ of qubits and can be read out by quantum measurements after a single-round time $t = \tau$. Within the total time T, the number of repetitive rounds of sensing and measurement is $\nu = T/\tau$. The standard deviation for any unbiased estimator $\hat{\chi}$ is bounded from below by the quantum Cramér–Rao bound (QCRB) [36,37],

$$\delta\hat{\chi} \geqslant 1/\sqrt{\nu F}, \tag{B1}$$

where F is the QFI at $t = \tau$ or, equivalently,

$$\delta\hat{\chi}\sqrt{T} \geqslant 1/\sqrt{F/\tau}. \tag{B2}$$

Thus, finding the optimal input state and quantum measurement to maximize the QFI is a central problem in high-precision quantum sensing. In general, the QFI of χ associated with ρ_χ is defined by $F = \mathrm{Tr}(\rho_\chi L^2)$ [36,37], where Tr is the trace operation and L is the symmetric logarithmic derivative (SLD) operator, which is given by

$$\partial_\chi\rho_\chi = (\rho_\chi L + L\rho_\chi)/2. \tag{B3}$$

Usually, a signal accumulation process is a unitary quantum channel, which gives $\rho_\chi = U_\chi\rho_0U_\chi^\dagger$, where U_χ is a time- and χ-dependent unitary operator. It has been shown that, for a pure state in unitary quantum channels, the QFI can be obtained from the variance of a Hermitian operator

$\mathcal{H} = i(\partial_\chi U_\chi^\dagger)U_\chi$ in ρ_0, with [30,74–76]

$$F = 4(\langle \mathcal{H}^2 \rangle - \langle \mathcal{H} \rangle^2), \tag{B4}$$

where $\langle O \rangle := \mathrm{Tr}(\rho_0 O)$ for any operator O. For an ensemble of N qubits as the input state in a standard Ramsey experiment, the maximal QFI ($\propto N^2$) is obtained when ρ_0 is the GHZ state [30], and when the inputs are uncorrelated qubits, $F \propto N$. So the GHZ state gives the Heisenberg scaling for the sensing precision while the uncorrelated inputs leads to the SQL, according to Eq. (B2). However, in the presence of noise, the unitary quantum channel will be modified by errors, and the corresponding QFI will be reduced or even be lost. As a result, the expected sensing precision may not be achieved.

A special case is taking the quantity χ to be the relative phase ϕ of the two interferometric modes, and the unitary phase imprinting operator is given by $U_\phi = \exp(-i\phi J_z)$, where $J_z = \sum_{i=1}^N \sigma_{iz}/2$ is half of the relative number operator between the two modes. And the corresponding $\mathcal{H}$ in Eq. (B4) is $\mathcal{H} = J_z$. Therefore, the QFI in Eq. (B4) is exactly the variance of the relative number with respect to the initial probe state, and the QCRB in Eq. (B1) manifests itself as the uncertainty relation between the *relative* phase and the *relative* number (take $\nu = 1$). So the initial state with the largest relative number fluctuation (e.g., the GHZ state) gives the highest phase resolution, while the total number of the state can be fixed.

APPENDIX C: CALCULATIONS OF THE NOISY QUANTUM FISHER INFORMATION UNDER INDEPENDENT DEPHASING

Here we give the detailed calculations of the noisy QFI under independent dephasing and generalize the result for Sagnac-type interferometers to more genetic classes. The spectral decomposition of the density matrix ρ is given by

$$\rho = \sum_{i=1}^{d} p_i |\psi_i\rangle\langle\psi_i|, \tag{C1}$$

where d is the dimension of the support set of ρ, and p_i is the ith eigenvalue of ρ, with $|\psi_i\rangle$ being the corresponding ith eigenvector. With this representation, the QFI with respect to the quantity χ can be expressed as [77,78]

$$F = \sum_{i=1}^{d} \frac{(\partial_\chi p_i)^2}{p_i} + \sum_{i=1}^{d} 4p_i \langle \partial_\chi \psi_i | \partial_\chi \psi_i \rangle - \sum_{\substack{i,j=1; \\ p_i+p_j\neq 0}}^{d} \frac{8p_i p_j}{p_i + p_j} |\langle \psi_i | \partial_\chi \psi_j \rangle|^2. \tag{C2}$$

For the readout GHZ state

$$\rho(\tau) = [|\mathbf{0}\rangle\langle\mathbf{0}| + |\mathbf{1}\rangle\langle\mathbf{1}| + (e^{-N\gamma\tau} e^{i\phi_S} |\mathbf{0}\rangle\langle\mathbf{1}| + \mathrm{H.c.})]/2 \tag{C3}$$

at $t = \tau$, where $\phi_S = \beta N \Omega \tau^2$ is the Sagnac phase, the dimension of the support set is $d = 2$, with the two eigenvalues $p_\pm = (1 \pm e^{-N\gamma\tau})/2$ and the corresponding eigenvectors $|\psi_\pm\rangle = (e^{i\phi_S}|\mathbf{0}\rangle \pm |\mathbf{1}\rangle)/\sqrt{2}$, respectively. The QFI with respect to the rotation frequency Ω can be readily calculated from Eq. (C2) and is given by

$$F = \left(\frac{\partial \phi_S}{\partial \Omega}\right)^2 e^{-2N\gamma\tau} = \beta^2 N^2 \tau^4 e^{-2N\gamma\tau}, \tag{C4}$$

which is Eq. (10) in the main text. In noiseless scenarios with $\gamma = 0$, F/τ increases monotonically with τ while it has an optimum for finite dephasing strength. In Fig. 4 we show the effects of increasing the dephasing strength on the interrogation-time-normalized QFI of the readout state with a fixed qubit number N. One sees that both of the optimal F/τ and optimal interrogation time are decreasing with increasing γ.

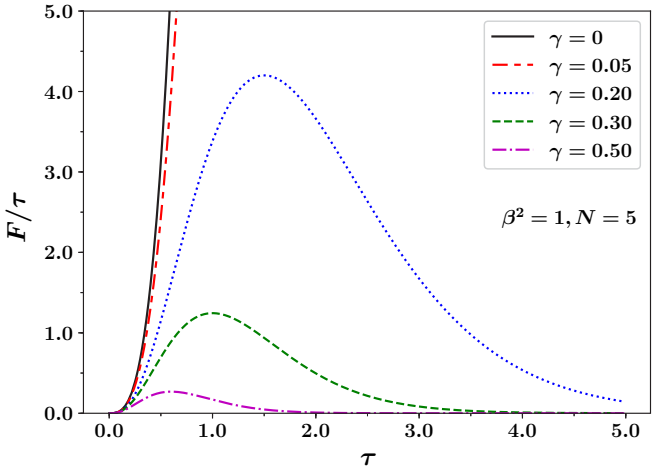

FIG. 4. Effects of increasing the dephasing strength γ on F/τ vs τ. We set $\beta^2 = 1$ and the representative value for the qubit number is $N = 5$.

1. Quantum Fisher information of generic matter-wave interferometry schemes.

For generic MWI schemes with GHZ states and under independent dephasing noise, if the accumulated phase is $\phi_\chi(\tau) \propto N\chi\tau^\lambda$ ($\lambda > 0$), then following the same procedure one can easily obtain the QFI with respect to the quantity χ, which is given by

$$F_\chi = \left(\frac{\partial \phi_\chi}{\partial \chi}\right)^2 e^{-2N\gamma\tau} \propto N^2 \tau^{2\lambda} e^{-2N\gamma\tau}. \tag{C5}$$

And the interrogation-time optimized value of F_χ/τ is $(F_\chi/\tau)_{\mathrm{opt}} = O(N^{3-2\lambda})$, with $\tau_{\mathrm{opt}} = (2\lambda - 1)/(2N\gamma)$. So for $\lambda \geqslant 1$, the best QFI that can be achieved is $(F_\chi/\tau)_{\mathrm{opt}} = O(N)$ (SQL) with the $\lambda = 1$ class. See main text.

[1] C. L. Degen, F. Reinhard, and P. Cappellaro, Rev. Mod. Phys. **89**, 035002 (2017).

[2] V. Giovannetti, S. Lloyd, and L. Maccone, Science **306**, 1330 (2004).

[3] V. Giovannetti, S. Lloyd, and L. Maccone, Phys. Rev. Lett. **96**, 010401 (2006).

[4] B. Barrett, R. Geiger, I. Dutta, M. Meunier, B. Canuel, A. Gauguet, P. Bouyer, and A. Landragin, C. R. Phys. **15**, 875 (2014).

[5] M. Kasevich and S. Chu, Phys. Rev. Lett. **67**, 181 (1991).

[6] T. L. Gustavson, P. Bouyer, and M. A. Kasevich, Phys. Rev. Lett. **78**, 2046 (1997).

[7] M. C. Kandes, R. Carretero-Gonzalez, and M. W. J. Bromley, arXiv:1306.1308.

[8] R. Trubko, J. Greenberg, M. T. S. Germaine, M. D. Gregoire, W. F. Holmgren, I. Hromada, and A. D. Cronin, Phys. Rev. Lett. **114**, 140404 (2015).

[9] J. L. Helm, S. L. Cornish, and S. A. Gardiner, Phys. Rev. Lett. **114**, 134101 (2015).

[10] S. A. Haine, Phys. Rev. Lett. **116**, 230404 (2016).

[11] J. L. Helm, T. P. Billam, A. Rakonjac, S. L. Cornish, and S. A. Gardiner, Phys. Rev. Lett. **120**, 063201 (2018).

[12] R. Stevenson, M. R. Hush, T. Bishop, I. Lesanovsky, and T. Fernholz, Phys. Rev. Lett. **115**, 163001 (2015).

[13] C. Luo, J. Huang, X. Zhang, and C. Lee, Phys. Rev. A **95**, 023608 (2017).

[14] S. F. Huelga, C. Macchiavello, T. Pellizzari, A. K. Ekert, M. B. Plenio, and J. I. Cirac, Phys. Rev. Lett. **79**, 3865 (1997).

[15] B. M. Escher, R. L. de Matos Filho, and L. Davidovich, Nat. Phys. **7**, 406 (2011).

[16] R. Demkowicz-Dobrzański, J. Kołodyński, and M. Guţă, Nat. Commun. **3**, 1063 (2012).

[17] Q.-S. Tan, Y. Huang, X. Yin, L.-M. Kuang, and X. Wang, Phys. Rev. A **87**, 032102 (2013).

[18] J. Liu and H. Yuan, Phys. Rev. A **96**, 012117 (2017); **96**, 042114 (2017).

[19] E. M. Kessler, I. Lovchinsky, A. O. Sushkov, and M. D. Lukin, Phys. Rev. Lett. **112**, 150802 (2014).

[20] W. Dür, M. Skotiniotis, F. Fröwis, and B. Kraus, Phys. Rev. Lett. **112**, 080801 (2014).

[21] T. Unden, P. Balasubramanian, D. Louzon, Y. Vinkler, M. B. Plenio, M. Markham, D. Twitchen, A. Stacey, I. Lovchinsky, A. O. Sushkov, M. D. Lukin, A. Retzker, B. Naydenov, L. P. McGuinness, and F. Jelezko, Phys. Rev. Lett. **116**, 230502 (2016).

[22] We assume the total number of particles is fixed. For quantum sensing with states of a fluctuating total number of particles, see Ref. [69], where the precision bound is given by the average number of particles.

[23] J. J. Bollinger, W. M. Itano, D. J. Wineland, and D. J. Heinzen, Phys. Rev. A **54**, R4649 (1996).

[24] D. Leibfried, M. D. Barrett, T. Schaetz, J. Britton, J. Chiaverini, W. M. Itano, J. D. Jost, C. Langer, and D. J. Wineland, Science **304**, 1476 (2004).

[25] K. Mølmer and A. Sørensen, Phys. Rev. Lett. **82**, 1835 (1999).

[26] C. Lee, Phys. Rev. Lett. **97**, 150402 (2006).

[27] K. Gietka, P. Szańkowski, T. Wasak, and J. Chwedeńczuk, Phys. Rev. A **92**, 043622 (2015).

[28] L. Pezzé and A. Smerzi, Phys. Rev. Lett. **102**, 100401 (2009).

[29] M. Saffman and K. Mølmer, Phys. Rev. Lett. **102**, 240502 (2009).

[30] S. Pang and T. A. Brun, Phys. Rev. A **90**, 022117 (2014).

[31] C. J. Bordé, Phys. Lett. A **140**, 10 (1989).

[32] C. C. Gerry and J. Mimih, Phys. Rev. A **82**, 013831 (2010).

[33] P. L. Halkyard, M. P. A. Jones, and S. A. Gardiner, Phys. Rev. A **81**, 061602 (2010).

[34] F. Dalfovo, S. Giorgini, L. P. Pitaevskii, and S. Stringari, Rev. Mod. Phys. **71**, 463 (1999).

[35] The interrogation time τ is defined at which the center of the two counter-propagating Gaussian wave packets are completely overlapped (see Appendix A).

[36] C. W. Helstrom, *Quantum Detection and Estimation Theory* (Academic Press, New York, 1976).

[37] A. S. Holevo, *Probabilistic and Statistical Aspects of Quantum Theory* (North-Holland Publishing Company, Amsterdam, 1982).

[38] Here for Sagnac interferometers, the inter-path interaction is zero, which is different from Refs. [42,70,71], where the intra- and inter-modes interactions are almost canceled and the net interaction could be negligibly small in the phase imprinting process.

[39] D. Aghamalyan, M. Cominotti, M. Rizzi, D. Rossini, F. Hekking, A. Minguzzi, L.-C. Kwek, and L. Amico, New J. Phys. **17**, 045023 (2015).

[40] M. Kolář, T. Opatrný, and K. K. Das, Phys. Rev. A **92**, 043630 (2015).

[41] M. O. Scully and M. S. Zubairy, *Quantum Optics* (Cambridge University Press, Cambridge, 1997), p. 163.

[42] P. Szańkowski, M. Trippenbach, and J. Chwedeńczuk, Phys. Rev. A **90**, 063619 (2014).

[43] R. R. Puri and G. S. Agarwal, Phys. Rev. A **45**, 5073 (1992).

[44] T. W. Chen and P. T. Leung, Phys. Rev. A **67**, 055802 (2003).

[45] For each atom, we consider the fluctuation of the density-distribution dependent interaction [see Eq. (2)] or thermal fluctuations as the cause of the dephasing. The total dephasing operator is given by the summation over the individual qubits, where in Eq. (9) we have assumed the same dephasing strength γ for each atom for simplicity. This is different from the external-field-fluctuation-induced collective dephasing; e.g., for Ramsey-type interferometers, see Refs. [42,58,59]. Also, this is distinct from the periodical phase diffusion-revival process of single-particle coherence arising from nonlinear interactions with initial coherent spin states; e.g., see Ref. [72]. Such an evolution process does not diffuse the phase of the GHZ state and the reduced single-particle coherence always vanishes.

[46] Applying the $\pi/2$ pulse does not change the QFI with respect to Ω, so here we refer the state just after the Sagnac phase encoding as the readout state.

[47] Here we assume the Markovian noise. If considering the non-Markovian dephasing, then $\tau_{\rm opt} \propto 1/\sqrt{N}$ [73] and $(F/\tau)_{\rm opt} \propto \sqrt{N}$ for Sagnac-type interferometers.

[48] S. Pang and A. N. Jordan, Nat. Commun. **8**, 14695 (2017).

[49] T. Gefen, F. Jelezko, and A. Retzker, Phys. Rev. A **96**, 032310 (2017).

[50] M. Kasevich and S. Chu, Appl. Phys. B: Photophys. Laser Chem. **54**, 321 (1992).

[51] W. P. Schleich, D. M. Greenberger, and E. M. Rasel, Phys. Rev. Lett. **110**, 010401 (2013).

[52] W. P. Schleich, D. M. Greenberger, and E. M. Rasel, New J. Phys. **15**, 013007 (2013).
[53] M. Kritsotakis, S. S. Szigeti, J. A. Dunningham, and S. A. Haine, Phys. Rev. A **98**, 023629 (2018).
[54] T. L. Gustavson, A. Landragin, and M. A. Kasevich, Classical Quantum Gravity **17**, 2385 (2000).
[55] D. S. Durfee, Y. K. Shaham, and M. A. Kasevich, Phys. Rev. Lett. **97**, 240801 (2006).
[56] Note that if one fixes the initial kicking angular momentum L_k while doing the optimization, then the scheme will belongs to the $\lambda = 1$ class, as in Ref. [33].
[57] G. Ferrini, D. Spehner, A. Minguzzi, and F. W. J. Hekking, Phys. Rev. A **84**, 043628 (2011).
[58] U. Dorner, New J. Phys. **14**, 043011 (2012).
[59] W. Zhong, Z. Sun, J. Ma, X. Wang, and F. Nori, Phys. Rev. A **87**, 022337 (2013).
[60] P. Schindler, J. T. Barreiro, T. Monz, V. Nebendahl, D. Nigg, M. Chwalla, M. Hennrich, and R. Blatt, Science **332**, 1059 (2011).
[61] G. Waldherr, Y. Wang, S. Zaiser, M. Jamali, T. Schulte-Herbrüggen, H. Abe, T. Ohshima, J. Isoya, J. F. Du, P. Neumann, and J. Wrachtrup, Nature (London) **506**, 204 (2014).
[62] N. Ofek, A. Petrenko, R. Heeres, P. Reinhold, Z. Leghtas, B. Vlastakis, Y. Liu, L. Frunzio, S. M. Girvin, L. Jiang, M. Mirrahimi, M. H. Devoret, and R. J. Schoelkopf, Nature (London) **536**, 441 (2016).
[63] G. Arrad, Y. Vinkler, D. Aharonov, and A. Retzker, Phys. Rev. Lett. **112**, 150801 (2014).
[64] X.-M. Lu, S. Yu, and C. H. Oh, Nat. Commun. **6**, 7282 (2015).
[65] R. Ozeri, arXiv:1310.3432.
[66] F. Reiter, A. S. Sørensen, P. Zoller, and C. A. Muschik, Nat. Commun. **8**, 1822 (2017).
[67] R. Demkowicz-Dobrzański, J. Czajkowski, and P. Sekatski, Phys. Rev. X **7**, 041009 (2017).
[68] S. Zhou, M. Zhang, J. Preskill, and L. Jiang, Nat. Commun. **9**, 78 (2018).
[69] P. Hyllus, L. Pezzé, and A. Smerzi, Phys. Rev. Lett. **105**, 120501 (2010).
[70] M. F. Riedel, P. Böhi, Y. Li, T. W. Hänsch, A. Sinatra, and P. Treutlein, Nature (London) **464**, 1170 (2010).
[71] C. Gross, T. Zibold, E. Nicklas, J. Estève, and M. K. Oberthaler, Nature (London) **464**, 1165 (2010).
[72] Y. Khodorkovsky, G. Kurizki, and A. Vardi, Phys. Rev. A **80**, 023609 (2009).
[73] A. W. Chin, S. F. Huelga, and M. B. Plenio, Phys. Rev. Lett. **109**, 233601 (2012).
[74] S. Boixo, S. T. Flammia, C. M. Caves, and J. M. Geremia, Phys. Rev. Lett. **98**, 090401 (2007).
[75] M. M. Taddei, B. M. Escher, L. Davidovich, and R. L. de Matos Filho, Phys. Rev. Lett. **110**, 050402 (2013).
[76] J. Liu, X.-X. Jing, and X. Wang, Sci. Rep. **5**, 8565 (2015).
[77] Y. M. Zhang, X. W. Li, W. Yang, and G. R. Jin, Phys. Rev. A **88**, 043832 (2013).
[78] J. Liu, X.-X. Jing, W. Zhong, and X. Wang, Commun. Theor. Phys. **61**, 45 (2014).